Turkish Journal of Remote Sensing

https://dergipark.org.tr/en/pub/tuzal

e-ISSN 2687-4997

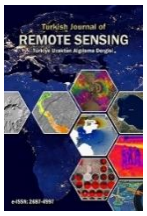

Comparison of DEM based on Geodetic Methods and Photogrammetric Usage of UAV

Hasan Bilgehan Makineci*[1], Hakan Karabörk [1], Akif Durdu [2]

[1]Konya Technical University, Engineering and Nature Sciences Faculty, Department of Geomatics Engineering, Konya, TURKIYE
[2]Konya Technical University, Engineering and Nature Sciences Faculty, Department of Electrical and Electronical Engineering, Konya, TURKIYE

Keywords
Accuracy Assesment
DEM
SfM
UAV

ABSTRACT

Unmanned Aerial Vehicles (UAV) use in the production of the map for photogrammetric purposes. Unlike aerial photogrammetry, UAV cameras are non-metric amateur cameras. Therefore, they need some operations to use in photogrammetry. Structure from Motion (SfM) algorithms prefers for processing images because of the usage of the non-metric cameras. These algorithms generally identify key-points (via feature extraction) on the photos and match tie-points (via feature point matching) in overlap images. SfM is a photogrammetric technique that produces keypoint to match by identifying key points, such as edge-to-corner points, through high-resolution RGB photos. The scope of this study was to compare the results obtained by UAVs and the results acquired by ground truth data. In this comparison, SfM algorithm performance, the effects of flight height, overlap rate, and UAV-type on the model investigated, and significant results achieved. Additionally, the models obtained from the UAV photographs with different flight heights and overlaps in the areas with varying characteristics of the slope compared. Consequently, it determined the difference between around 20 cm (Z value), comparing the flight height of 80 m and the flight height of 120 m. Since it is observed that the flight height does not have a significant effect.

Jeodezik Tekniklerle ve İHA'nın Fotogrametrik Kullanımı ile Üretilen Sayısal Yükseklik Modellerinin Karşılaştırılması

Anahtar Kelimeler
Doğruluk Araştırması
İHA
SfM
SYM

Öz

Son yıllarda fotogrametrik amaçlı harita üretiminde İnsansız Hava Araçları (İHA) sıklıkla kullanılmaktadır. Hava fotogrametrisinde kullanılan kameraların aksine, İHA kameraları metrik olmayan kameralardır. Bu nedenle fotogrametride kullanmak için bazı işlemlere ihtiyaç duyarlar. 3 Boyutlu model üretiminde kameranın farklı pozisyonlardan bindirmeli fotoğraf çekimi esasına dayalı Structure from Motion (SfM) algoritmaları, metrik olmayan kameraların kullanılmasına olanak sağlamaktadır. Bu algoritmalar genellikle fotoğraflardaki anahtar noktaları (öznitelik çıkarma yoluyla) tanımlar ve bindirmeli görüntülerde bağlantı noktalarını (öznitelik noktası eşleştirmesi yoluyla) eşleştirir. SfM, yüksek çözünürlüklü fotoğraflar aracılığıyla kenar noktaları köşe noktaları gibi kilit noktaları (keypoint) tanımlayarak eşleşecek anahtar nokta (tie point) üreten bir fotogrametrik tekniktir. Bu çalışmanın amacı, İHA'lar ile çekilmiş fotoğraflardan 3B model üreterek, arazi verilerinden elde edilen 3B modelin karşılaştırılmasıdır. Bu karşılaştırmada SfM algoritma performansı, uçuş yüksekliği, bindirme oranı ve İHA türünün model üzerindeki etkileri incelenmiş ve önemli sonuçlar elde edilmiştir. Ayrıca farklı uçuş yüksekliklerine sahip İHA fotoğraflarından elde edilen modeller ve farklı eğim özelliklerine sahip arazilerde de karşılaştırmalar gerçekleştirildi. Sonuç olarak 80 m uçuş yüksekliği ile 120 m uçuş yüksekliği arasındaki farkın (en büyük fark olarak) 20 cm olduğu (Z değerinde) tespit edilmiştir.

* **Corresponding Author**

*(hbmakineci@ktun.edu.tr) ORCID ID 0000-0003-3627-5826
(hkarabork@ktun.edu.tr) ORCID ID 0000-0001-7387-7004
(adurdu@ktun.edu.tr) ORCID ID 0000-0002-5611-2322

Cite this article

Makineci H B, Karabörk H & Durdu A (2020). Comparison of DEM based on Geodetic Methods and Photogrammetric Usage of UAV. Turkish Journal of Remote Sensing, 2(2), 58-69

Research Article

Received: 28/09/2020; Accepted: 17/10/2020

1. INTRODUCTION

Photogrammetry is defined as the method of measurement and evaluation through various images without contacting objects. Due to the high accuracy and faster mapping of large areas, the photogrammetry method preferred for many years. Metric cameras used in aerial photogrammetry have a significant effect on this accuracy (Martínez-Carricondo et al., 2018).

Unlike metric cameras used in aerial photogrammetry, UAV cameras (generally) are amateur cameras (non-metric). For this reason, they must pass through some stages to use in photogrammetry — UAVs commonly used in remote sensing in the last quarter-century. Compared to satellite and aircraft-based systems, repetitive measurement capacity offers significant advantages for users in terms of data production with low cost and very high resolution (Comert. et al., 2019). One of the crucial reasons for the increase of the photogrammetric usage of UAVs is the increase in the use of highly self - executing software. This software offers high model accuracy and easy-to-use user-friendly methods. In particular, the evaluation of the final products of end-user software is an essential issue for researchers (Cryderman et. al., 2014, Draeyer and Christoph 2014, Strecha, 2014).

Unmanned Aerial Vehicle (UAV) is called a plane that does not carry any pilot or people and command remotely. UAV provides outstanding contributions to fast and up-to-date data collection. It is necessary to determine the accuracy of these products obtained in these low-cost systems (Uysal, M., et al., 2018). Scientific researches carried out through UAVs can be considered very new. In contrast to military studies, the use of UAV for civil purposes has increased remarkably over the last decade (Mesas-Carrascosa, et. al. 2014, Colomina and Pere 2014). UAVs including photogrammetric digital elevation model (DEM) production, agricultural research, and applications (Berni, J., AJ., et al., 2009), transportation (Martínez-Carricondo, P., et al., 2018, Amukele, T. K., et al., 2015), architectural studies, environmental factors, monitoring, emergency and disaster situations, technological research, entertainment, and education sector and more others nowadays, it is used in almost every different branches.

Considering that the production costs are low, the model accuracy produced by UAVs is higher than expected (Cryderman, C., et. Al., 2014). The latest research shows that the accuracy of the position of the products produced by UAVs with the new technology is well above the expectations. According to RTK-GNSS based measurement results, DEM with a point density of 35 points/ha and UAV DEM, whose point density calculated as 235 points/ha, were compared, when UAV-based DEM used as the reference plane, the volumes of excavations found to be very close to each other (Akgul, M., et al., 2018).

Despite the negativities such as short flight distances, low battery life, and insufficient camera resolutions in general, UAVs are found successful and sufficient by the researchers. The recent development and research activities are so intensive on this issue and that it is expected to perform a much more critical role in the future (Cryderman, C., et. Al., 2014, Mesas-Carrascosa, F. J., et al., 2014, Berni, J. AJ., et al., 2014, Martínez-Carricondo, P., et al., 2018, Amukele, T. K., et al., 2015).

UAVs are mainly composed of 3 components (Colomina, I., and Pere M.., 2014, Arik, S., et. Al., 2018). The first and most crucial component is the main body. In this section, the engine, battery, wing are inside (vital mechanical equipment for flight). The second component includes the whole the electronic sensors that calculate the aircraft's positional status, angular velocity and linear acceleration (such as a gyroscope). The latest component is the sensors that are preferred by the users. For public use as a payload, RGB cameras are the most preferred sensors. Sensors that can obtain images in different bands (Near Infrared, Infrared, Radar, Sonar, Thermal Sensors, Multispectral Sensors, Hyperspectral Sensors, etc.) (Sabins, F., 2007) can be used for different goals if preferred by the users.

Model-generating software from UAV photographs generally produces results via a mathematical algorithm that base on the structure (known as "Structure from Motion"-SfM) (Carr, B. B., et al., 2019, Strecha, C., 2014). This algorithm focus on the combination of photographs taken from points with different bases with common matching points. In general, point matching algorithms in the literature such as FAST, SURF, ORB most commonly used methods (Govender, N., 2009). Also, In order to evaluate the reproducibility of a 3D model based on a UAV platform and structure-from-Motion algorithms, research frequently examined areas described by gentle slopes, with sets of ground control points. The mean absolute error tested by SfM is only 0.06 m (Clapuyt, F., et. al., 2016).

The cartographic representation of elevation data, which represents a specific part of a land, is divided into a grid, is called the Digital Elevation Model (DEM). DEM can proceed in many different ways. From stereo satellite images, interferometric SAR (InSAR) technique, stereo aerial photographs, and more other. It is possible to create DEM with many different techniques (Makineci, H. B., and Karabörk., H., 2016).

There are some struggles with the UAV flight plan examination. A study accompanied to review the effects of several altitudes and UAV types on the UAV-SfM based model correctness. It is illustrated to use UAVs for creating model aim relevant requirements (Yurtseven, H., 2019). Our study aimed to compare the results produced with the UAVs and the results produced by ground measurements and to determine the height differences between them. For this purpose, models of different types of terrain

(high slope area, sloping area, and flat field), different types of UAVs (fixed-wing and rotary vanes), and different flight parameters (flight height and overlap rates) produced. DEM has also been produced in the field by measurements (Real Time Kinematic RTK Method). By comparing the data of these two methods, accuracy analysis performed on the height differences of the points from sea level. To interpret the differences statistically and to be evaluated more quickly, a normal distribution was applied, three sigma rules applied, and the points outside the 95% confidence interval were determined — the effects of a normal distribution on accuracy investigated by subtracting the points outside the confidence interval. Also, points classified according to different field types and the effect of the slope on accuracy found. All results were interpreted, and the correlation between the models investigated.

2. METHOD

2.1. Used Unmanned Aerial Vehicles and Cameras

UAVs used to produce models are of two different types (Fig. 1). SenseFly eBee Plus model was used as fixed-wing UAV. The camera has a S.O.D.A (RGB) camera with the plugged camera. The fixed-wing UAV with a wingspan of 96 cm weighs about 700 gr. and can remain in the air for 50 minutes according to the factory data. For the fixed-wing UAV with integrated GNSS IMU systems, the wind resistance is specified as a maximum of 12 m / s. For the camera plugged on it, for S.O.D.A, the manufacturer is given 20-megapixel RGB sensor and 2.9 cm/pixel Ground Sample Distance (GSD) (for AGL 122 m flight height).

Figure 1. DJI Phantom 4 Pro Rotary Wing UAV and Integrated RGB Camera and SenseFly Ebee Fixed Wing UAV and RGB Camera S.O.D.A

DJI Phantom 4 Pro was used as the rotating winged UAV. An integrated RGB camera is used as a camera. This UAV has a wingspan of 35 cm (diagonal size) and weighs 1380 gr. In addition, according to the manufacturer's data, the wind resistance of the UAV which can remain in the air for 30 minutes is stated as 10 m/s. Features of the integrated camera are given as 20-megapixel RGB sensor and 3.33 cm/pixel Ground Sample Distance (GSD) (for AGL 122 m flight height). The rotary wing UAV with GNSS IMU systems is one of the most well-known industrially known brands worldwide. Table 1 shows the characteristics of the UAVs and cameras.

Table 1. Specs of the UAVs and cameras

UAV Name and Model	UAV Type	Camera Resolution	Wind Resis.	Max. Flight Time	Flight Speed Range
SenseFly Ebee	Fixed Wing	20 Megapixel	12 (m/s)	~50 min.	11-25 m/s
DJI Phantom 4 Pro	Rotary Wing	20 Megapixel	10 (m/s)	~30 min.	3-16 m/s

2.2. Study Area

In order to carry out the field work, coordinates between 542000.00m E - 4179760.00m N (UTM Zone 36s), region near the Karapınar district of Konya was preferred. This region is a rural area and is usually an uninhabited land with no vegetation near the agricultural areas. It is an area where the gradients of the field are gradually occurring and have different slopes suitable for the study. As can be seen in Fig. 2, which shows slope transitions, sharp transitions are not seen much in the region.

Located to the Karapınar district, the area is given in Fig. 2 (green-hatched region) is approximately 40 hectares and the area around 2.55 km. The field measurements and the environmental account are shown in Fig. 2 with Google earth pro software.

2.3. Structure from Motion (SfM)

This recent photogrammetric technique produces points to match by identifying keypoints such as edge-to-corner points through high-resolution RGB photographs. It also determines the routes of the same points by producing these points in the following photos. In this way, it calculates the base size (detects movement). By combining this information, it produces a model in matched points. If images captured by a camera can be scaled, it is sufficient to detect motion to obtain a fixed object model (Micheletti, Natan, et. Al., 2015, Govender, N., 2009).

SfM requires point correlation between images. Marked points (keypoints) are selected from each image. For this, an algorithm such as the Kanade-Lucas-Tomasi (KLT) algorithm can be used (14). If the photo-acquisition centers are close to each other, this algorithm provides a high success. Unfortunately, when the photographing centers' distance increases there will be the possibility for problems. In this case, feature matching algorithms (SIFT, SURF, ORB, etc.) are used (Makineci, H. B., et

al., 2020). The basic principle of these algorithms is that they solve the epipolar geometry of the photographic axes where the camera is located. Any point in a photograph is associated with an epipolar line in the other camera and the scale (base distance) is determined. In all related photographs, conjugate points are identified and combined and a sequence is formed between the images. In this way, the motion of the images is determined.

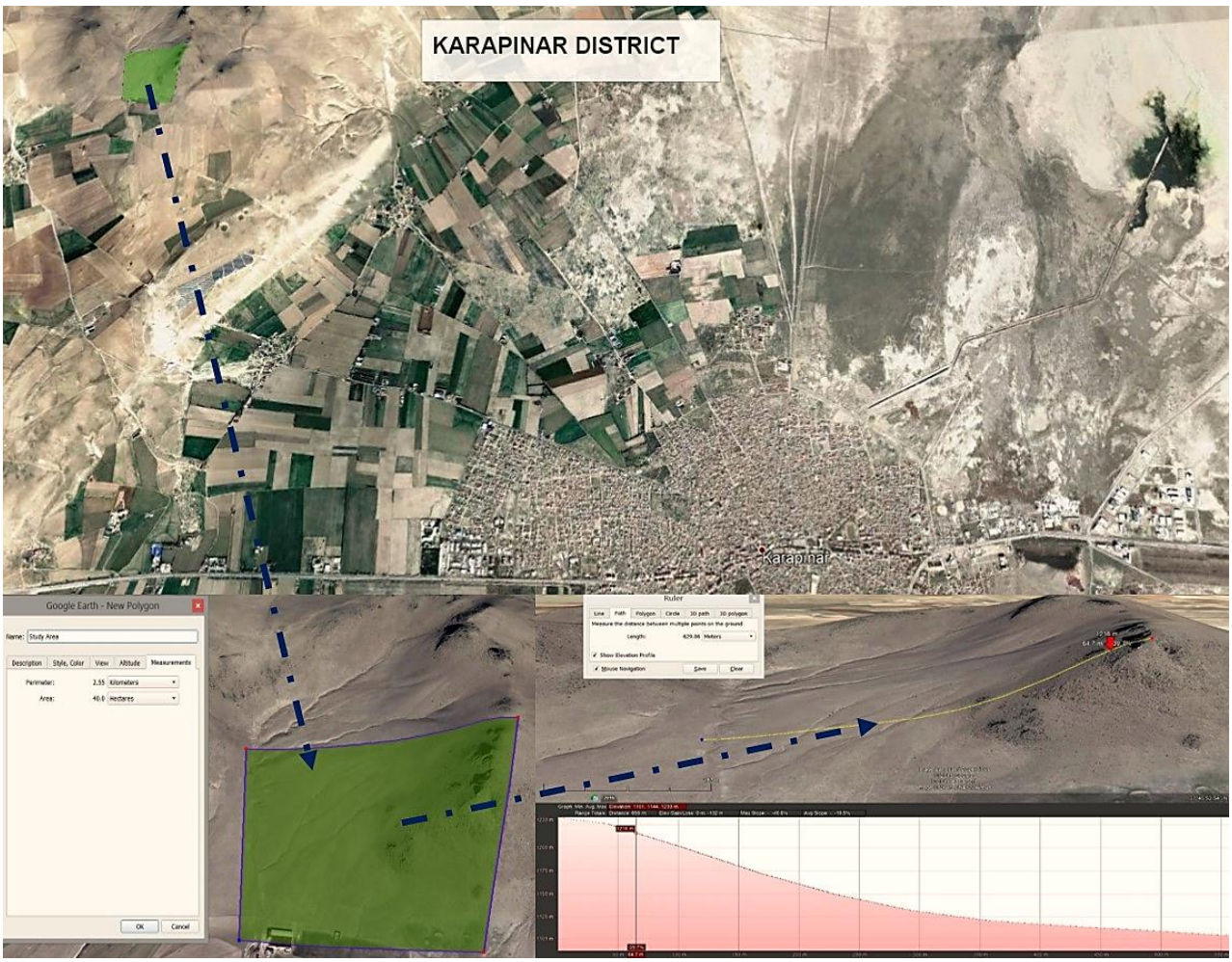

Figure 2. Working Area (Karapınar District and Study Area "green-hatched region") and Slope of Study Area

2.4. 3D Model Creation

Firstly, photos acquired based on photogrammetric basics (include with frontal overlap and side overlap) are import to the software (Pix4D). The following operations are done step by step automatically with the software.

• Photos merged, Key Points generated from each photo during this process (as described in SfM), Key Points produced in each photo matched with the related photos (tie point), and as a result, Sparse Cloud created.

• The points are densified and created "Dense Cloud" (the software performs the interpolation automatically).

• The surface is producing from Dense Cloud with triangulation (Mesh Model).

• Color values can be assigned and details to be clarified. The pictures are texturing to the surface model obtained from the dense cloud.

• In order to obtain a detailed texture, to obtain more accurate visualization, the surfaces are divided into pieces named tiled model (grid-grid network).

• Producing a regular grid piece (containing elevation data) representing a terrain (known as DEM).

• To determine transversal sections and longitudinal sections, to calculate volume-area calculations, contour lines produced.

• Orthomosaic produced that combines the entire photos.

• In addition to all these, if there are also Ground Control Points (GCP), it can be added to increase the accuracy of the model and to determine the accurate scale and coordinate transformations.

After the 3D model produced, the export can provide in different data formats. Intensive Point Data is exported as a point cloud and prepared for comparison with the points generated from the land. It can also export in DEM and Orthomosaic raster format. Users proceed to the accuracy analysis section through different alternatives. It is also possible to produce models with different operations based on these steps.

Three-sigma Rule

In the statistics, rule 68 - 95 - 99.7 (also called the empirical rule) is an estimation method used to determine the percentage of the values of the standard deviation widths between one and three that are within the normal distribution. According to the ranges, 68%, 95%, and 99% are one, two, and three standard deviations of the mean, sequentially (Gaikwad, L. M., et al., 2016). Notably, the normal distribution is shown in Fig 3 with the mean of the μ distribution and the standard deviation σ.

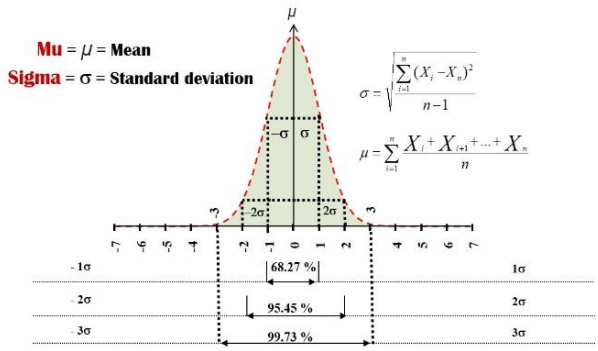

Figure 3. Three-sigma Rule

The Normal Distribution Analysis used to determine the coherence of the values and to eliminate the unpredictable measures called rough error. In general, an evaluation is made according to the number of data collected in scientific studies. If there are a large number of data, the values in the 99.7% confidence interval are analyzed by deducting the mean of 1 sigma (standard deviation) from the mean before evaluating. However, in the case of relatively few data, a 95% confidence interval (2 sigmas from the mean) is generally preferred in scientific research.

The standard deviation is a type of measure used to determine the variation, distribution, or trend of the group of values (Ahn., S., and J., A. F., 2003), as can be seen from Eq. (1); Standard Deviation is expressed by StD. ZR shows the elevation of the point from the reference data, and ZDEM shows the elevation of the point from the model.

$$Std=\sqrt{(\sum\_(i=1)\ ^n\text{▒}\ 〖(Z\_Ri-Z\_DEM_i)〗\ ^2/(n-1))} \quad (1)$$

The standard deviation and mean are the two most important values to determine the confidence interval. When performing the normal distribution analysis, a calculation is made for the 95% confidence interval, as in the Eq. (2). X stands for one value; μ means the mean value, and σ is the standard deviation.

a) $\mu-\sigma \leq X\_i \geq \mu+\sigma \cong 0.683$

b) $\mu-2\sigma \leq X\_i \geq \mu+2\sigma \cong 0.955$

c) $\mu-3\sigma \leq X\_i \geq \mu+3\sigma \cong 0.997$ (2)

2.5. Collecting Ground Truth Data

Photographs taken by UAVs were combined in software to produce DEM. A reference surface must use to investigate the accuracy of the produced model. Several field studies conducted to determine the surface of the ground (reference surface). The geoid roles as the fitting reference surface for height systems in the world-affirming orthometric heights. The production conditions of GCPs determined by following the " Photogrammetric Ground Works "section of the large scale map and map information production in Turkey. These GCPs fixed in square or circle format with a diameter of 3xGSD or an edge on the photo. Different colors of outer circles can create, and three or four arms of appropriate length can be marked to make the signs better visible. GCPs can be white or in contrasting colors with their surroundings. The sample GCP marked in the ground is shown in Fig. 4.

Figure 4. Sample of GCPs

Ground truth measurements (to produce a reference ground surface) were made by connecting the GNSS receiver to the Real Time Kinematic (RTK) method. A network of points of approximately 10 m intervals formed in the ground. More than thousand points measured, and the reference surface obtained — all points used for accuracy analysis for DEMs produced by UAV photographs. Thinking the atmospheric conditions, terrain types, and natural living conditions, making a positive effect on the flight plan. Timepieces, where atmospheric conditions were most appropriate, were determined as the flight hours when the sun rays did not fall perpendicular. Besides, many parameters such as wind, pressure, temperature, humidity, the location of GNSS satellites determined. A survey conducted on the hawk bird species in which habitat found in the region. All parameters were determined to be the most important day, time, and region determined by planning the flight.

Similar preferences were made for flight planning with fixed-wing UAV and with rotary-wing UAV to examine similar features of points. The

following chart (table 2) shows the average duration of the flights, the number of photographs taken, the Ground Sample Distance (GSD), and the total distance at which the UAV flies. In the same chart, flight planning features included.

Table 2. Flight plans and flight properties

Rotary Wing UAV										
Type	**Date**	**Flight Time**	**Area m^2 (m x m)**	**Frontal Overlap (%)**	**Side Overlap (%)**	**Camera Look Angle (°)**	**Flight Height (m)**	**Photo Count (Adet)**	**Perimeter (m)**	**Flight Duration (min)**
DJI Phantom 4 Pro	6.8.2018	12:22:29	515 x 560	70	63	90	100	337	5142	13:10
DJI Phantom 4 Pro	6.8.2018	12:49:23	515 x 560	80	72	90	100	604	6263	22:39
DJI Phantom 4 Pro	7.8.2018	10:02:57	515 x 560	80	72	90	120	416	5151	16:09
DJI Phantom 4 Pro	6.8.2018	14:28:40	515 x 560	70	63	90	80	568	6254	20:53
DJI Phantom 4 Pro	6.8.2018	17:21:48	515 x 560	70	63	90	90	268	6900	16:12
Fixed Wing UAV										
Type	**Date**	**Flight Time**	**Area m^2 (m x m)**	**Frontal Overlap (%)**	**Side Overlap (%)**	**Camera Look Angle (°)**	**Flight Height (m)**	**Photo Count (Adet)**	**Perimeter (m)**	**Flight Duration (min)**
Sense Fly Ebee RTK+	7.8.2018	11:52:00	510 x 560	80	65	90	120	176	15200	18:00
Sense Fly Ebee RTK+	8.8.2018	11:32:00	510 x 560	80	65	90	170	134	16500	18:00

2.6. Findings of Accuracy Assessment Analysis

As a result of the studies, a total of seven models DEM produced. In Fig. 5, all the models are shown together. Besides, the slope map produced to classify the points shown in Fig. 5. The points that acquired in the area found on

DEMs and the coordinates matched. Accuracy analyses performed by comparing the Z values of the points whose coordinates match in the area with the Z values determined from the DEM.

Figure 7 shows all of the ground truth points. In Fig. 6, ground truth points classified by slope classes. Each slope class has been evaluated separately for the evaluation of ground truth points by the slope.

All control-points obtained from the terrain matched with the elevation value corresponding to their horizontal coordinates (X - Y) and the differences calculated. The ground truth points on the generated models shown in Fig. 6. Also, ground points are classified according to the slope where they match (on the slope map), and these classes are shown in Fig. 6.

Accuracy assessments made for all points in the models (except for some points). The results of the accuracy assessment give in Table 3. The accuracy estimation for the models was determined by obtaining standard deviations from all points (including sharp points). The minimum and the maximum difference of each model are shown in the table. The average of the differences also infers in Table 3.

The evaluations included in Table 3 also contain the points that are analyzed to have rough errors. The accuracy analysis obtained by discarding the rough errored points from the accuracy assessment is given in Table 4.

In addition, Root Mean Square Error (RMSE) analysis was added to the study to make it more statistically significant. Since it is a frequently preferred method in DEM studies in the literature, $RMSE_z$ was calculated and interpreted in the results. In order to recognize the relationship between the points, the slope of the points is shown in Fig. 5. The accuracy analysis of the points classified according to the slopes produced from this figure also has to be performed. Table 5 shows the number of points, standard deviations, mean values, minimum and maximum values.

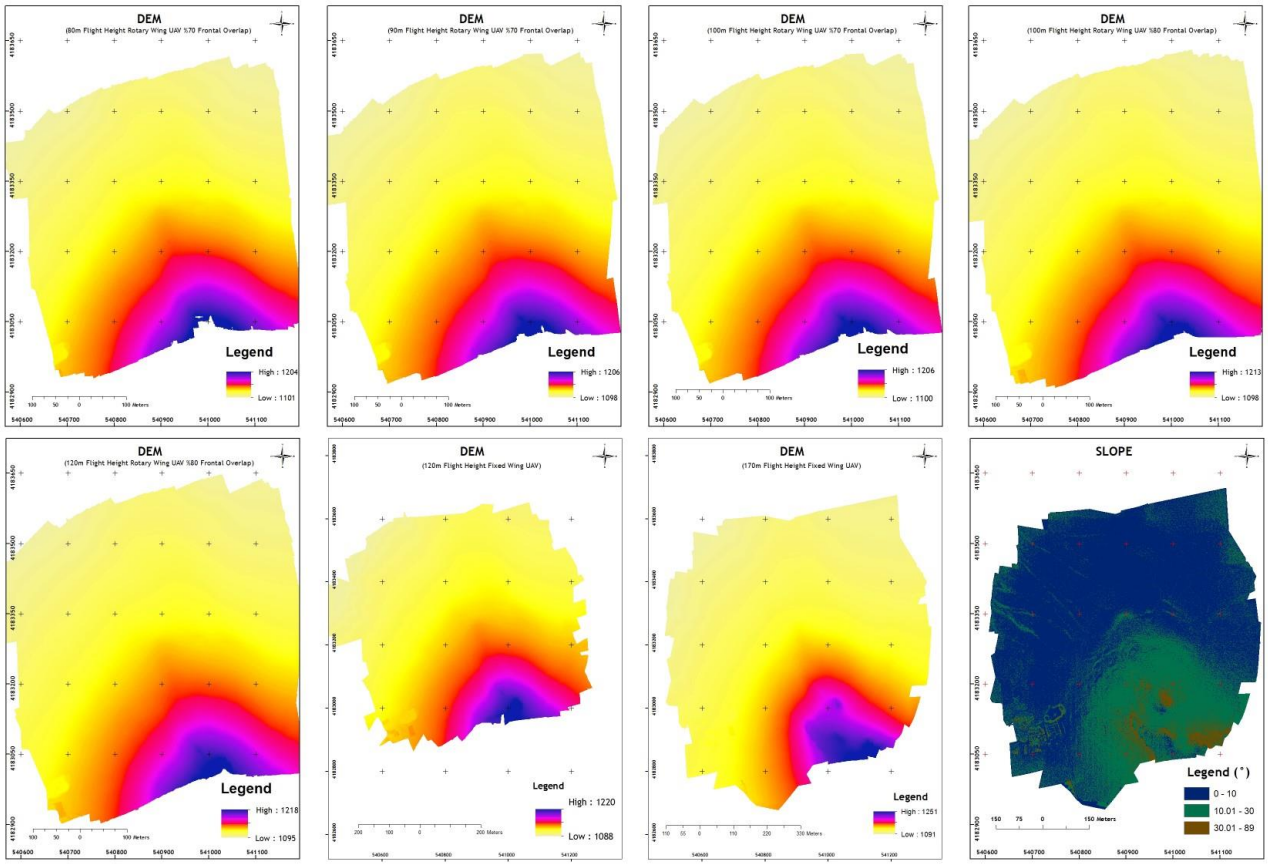

Figure 5. All DEMs Produced from Different Flight Plans and Slope Map Generated from DEMs

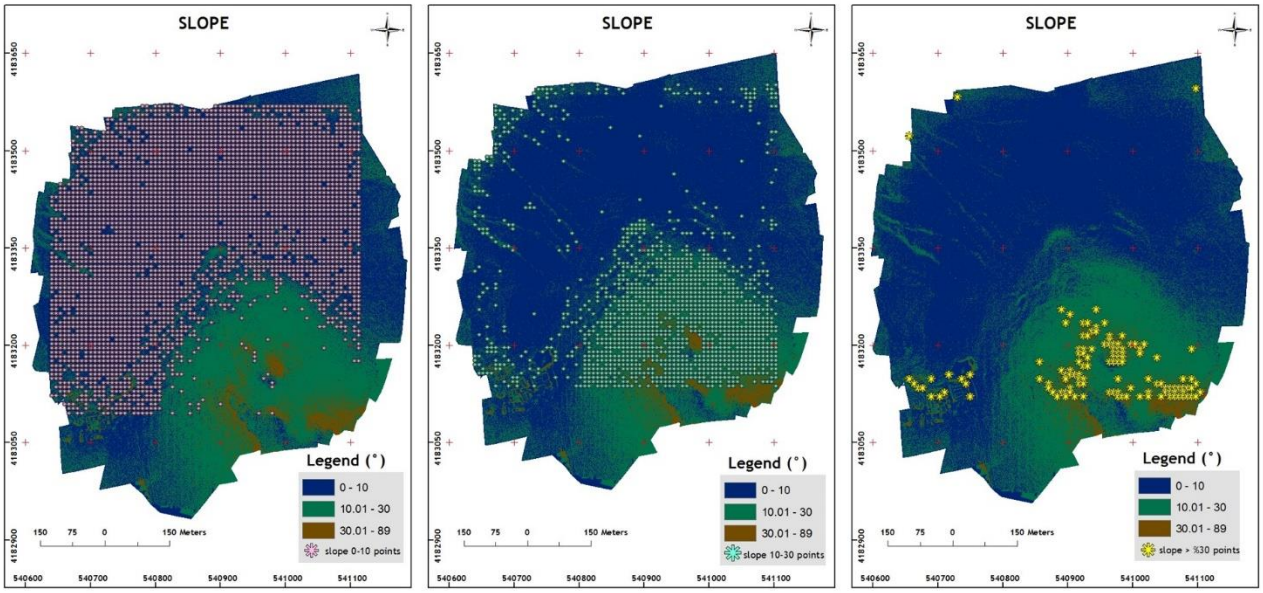

Figure 6. Classification and Illustration of Ground Truth Points on Various Slopes

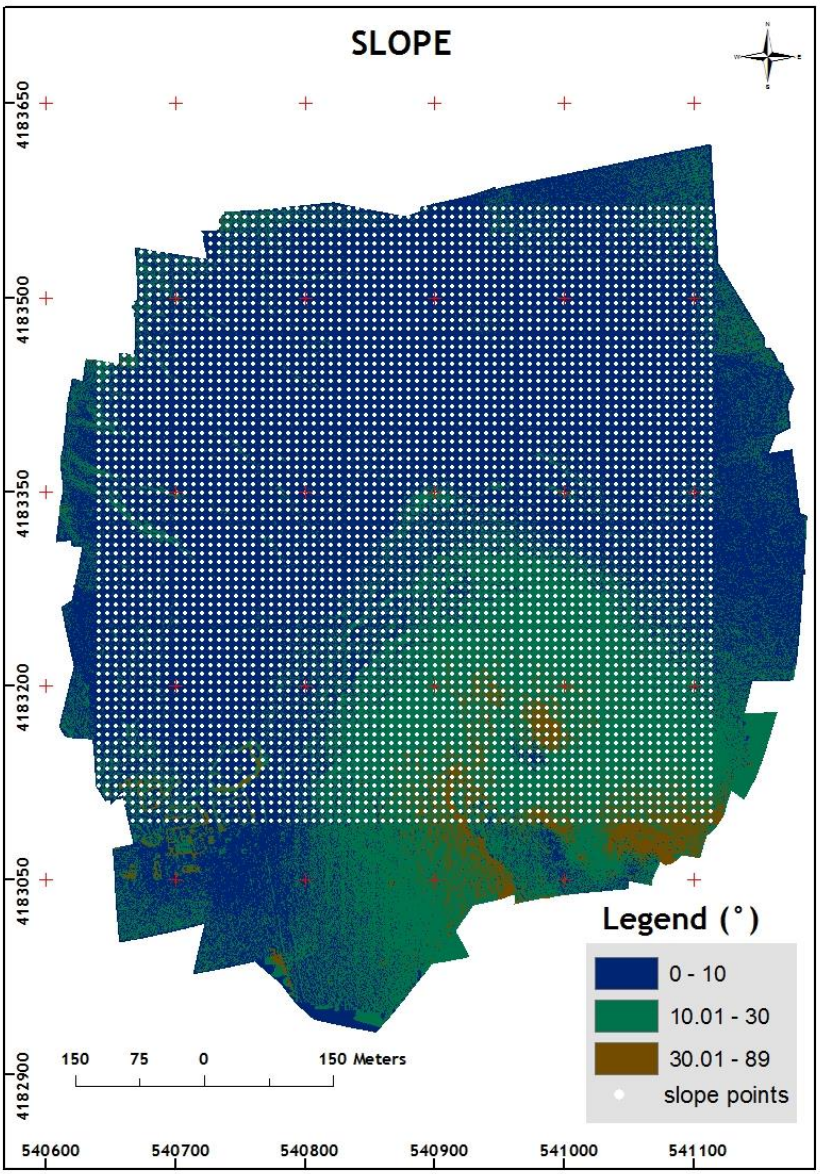

Figure 7. Distribution of Ground Truth Points on Slope Map

Table 3. Accuracy Assessment for All Points in The DEMs (including rough errored points)

Flight Type	*Standart Deviation (m)*	*Mean (m)*	*Max. (m)*	*Min. (m)*	*Points (Piece)*	*RMSE$_z$ (m)*
80 m Flight Height (AGL) Rotary Wing UAV (%70 frontal overlap)	1.18	1.2	11.3	-4.9	1188	1.57
90 m Flight Height (AGL) Rotary Wing UAV (%70 frontal overlap)	1.25	1.2	12.1	-5.0	1360	1.69
100 m Flight Height (AGL) Rotary Wing UAV (%70 frontal overlap)	1.19	1.2	12.3	-5.2	1319	1.66
100 m Flight Height (AGL) Rotary Wing UAV (%80 frontal overlap)	1.2	1.3	12.1	-5.0	1595	1.49
120 m Flight Height (AGL) Rotary Wing UAV (%80 frontal overlap)	1.21	1.4	12.0	-7.5	1801	1.60
120 m Flight Height (AGL) Fixed Wing UAV (%80 frontal overlap)	1.32	1.3	13.1	-7.6	1677	1.76
170 m Flight Height (AGL) Fixed Wing UAV (%80 frontal overlap)	1.67	1.6	12.0	-13.4	1025	2.01

Table 4. Accuracy Assessment for All Points in The DEMs (contains 95% Confidence Intervals)

Flight Type	*Standart Deviation (m)*	*Mean (m)*	*Max. (m)*	*Min. (m)*	*Points (Piece)*	*$RMSE_z$ (m)*
80 m Flight Height (AGL) Rotary Wing UAV (%70 frontal overlap)	0.78	1.2	6.5	-1.9	1052	1.04
90 m Flight Height (AGL) Rotary Wing UAV (%70 frontal overlap)	1.02	1.2	6.6	-2.0	1212	1.16
100 m Flight Height (AGL) Rotary Wing UAV (%70 frontal overlap)	0.96	1.2	6.5	-2.0	1177	1.11
100 m Flight Height (AGL) Rotary Wing UAV (%80 frontal overlap)	0.98	1.3	6.7	-2.1	1431	1.11
120 m Flight Height (AGL) Rotary Wing UAV (%80 frontal overlap)	1.0	1.4	6.1	-2.1	1561	1.12
120 m Flight Height (AGL) Fixed Wing UAV (%80 frontal overlap)	1.11	1.3	6.9	-2.6	1434	1.29
170 m Flight Height (AGL) Fixed Wing UAV (%80 frontal overlap)	1.23	1.6	7.5	-3.2	1741	1.52

Table 5. Accuracy Assessment of Classified Points in Slope Map

Slope Type (°)	Standart Deviation (m)	Mean (m)	Max. (m)	Min. (m)	Points (Piece)	$RMSE_z$ (m)
0 - 10	0.81	1.18	10.1	-2.1	1319	1.05
10.01 - 30	1.79	1.86	10.9	-7.6	1449	2.24
> 30	2.8	3.05	10.1	-2.1	322	4.72

3. RESULTS

To explain what has been done in practice of research section and make it remarkable, results-oriented explanations made in this section. It was written as a necessary part to relate results and objectives in the study and to reveal the findings. The results generally divided by terrain slope classes and confidence intervals. All classes illuminated step by step, and all explained separately.

A model that is 70% overlapping with a rotary-wing UAV from a height of 80 m (above ground) was produced. When the ground control points acquired from the land assessed with this DEM, the standard deviation determined as 1.18 m and $RMSE_z$ determined as 1.57 m. After the incoherent points eliminated from the model, which did not match the normal distribution curve (95% confidence interval). The standard deviation found 0.78 m and $RMSE_z$ determined as 1.04 m after the elimination of rough error points.

Second model that is 70% overlapping with a rotary-wing UAV from a height of 90 m (above ground) was produced. When the ground control points acquired from the land assessed with this DEM, the standard deviation determined as 1.18 m and $RMSE_z$ determined as 1.69m. After the incoherent points eliminated from the model, which did not match the normal distribution curve (95% confidence interval). The standard deviation found 1.02 m and $RMSE_z$ determined as 1.69 m after the elimination of rough error points.

The model produced from a flight height of 100 m (70% overlapped), with a rotary-winged UAV and 337 photos. The standard deviation determined as 1.19 m and $RMSE_z$ determined as 1.66 m. The rough errors identified and incoherent measurements eliminated from the model. The standard deviation found to be 0.96 m and $RMSE_z$ determined as 1.11 m in the accuracy assessment.

Another model produced from a flight height of 100m, with a rotary-winged UAV and an 80% overlapped 337 photos. The standard deviation was determined as 1.20 m when compared to DEM and the ground truth data. The so-called coarse error was determined, and incoherent points removed from the model. Then, the standard deviation found 0.98 m and $RMSE_z$ determined as 1.11 m.

From the height of 120m with an 80% overlap, another model produced with 416 photographs, with the rotary-winged UAV. The standard deviation determined as 1.21 m and RMSEz determined as 1.60 m. The rough errored points were determined and removed from the analysis. The standard deviation found 1.0 m and $RMSE_z$ determined as 1.12 m after the removal of rough errors. At the same flight height, another model produced with 604 photos (an 80% overlapped) obtained from the fixed-winged UAV. The standard deviation determined as 1.32 m and $RMSE_z$ determined as 1.76 m. The rough errors

identified and the incoherent points eliminated from the model. The standard deviation determined as 1.11 m and $RMSE_z$ determined as 1.29 m in this accuracy assessment.

Lastly, 170 m height (from the ground), a DEM produced with fixed-wing UAV, 80% overlapped 134 photos. The standard deviation determined as 1.67 m and $RMSE_z$ determined as 1.76 m. Incoherent points excluded from the system, which did not match the 95% confidence interval. The standard deviation found to be 1.23 m and $RMSE_z$ determined as 1.52 m.

According to slopes, the study area divided into three classes. One thousand three hundred nineteen points detected in the flat areas (0 - 10° slope) — the standard deviation value determined as 0.81 m and $RMSE_z$ determined as 1.05 m in flat areas. One thousand four hundred forty-nine points evaluated in the middle slope zone (10.01 - 30° slope), and as a result, 1.79 m standard deviation detected, and $RMSE_z$ determined as 2.24 m. Finally, three hundred twenty-two points determined in high slope areas (slope higher 30°). The standard deviation of 322 points found 2.8 m and $RMSE_z$ determined as 4.72 m.

4. DISCUSSION

As recognized from the charts, the coherence of the models with each other is powerful. The GCPs used in the creation steps of the models measured with GNSS (RTK) with tremendous accuracy. GCPs arranged for each DEM and coordinate transformations fitted with the corresponding points. Therefore, it is achievable to have confidential results for all models.

Thus, it achieved the difference between around 20 cm (for elevation line), analyzing the flight height of 80 m (with rotary-wing UAV), and the flight height of 120 m (with rotary-wing UAV). Since it is observed that the flight height does not have a significant effect, it is commented that it is not undesirable to fly high in projects that do not require very high result accuracy. As a general idea, it was determined that the photos taken with a high overlap rate and the flights made from low altitudes do not have a high impact on model accuracy.

The accuracy mentioned for UAVs in general literature is higher. However, the final product accuracy may have been affected because the research was carried out in an area where the terrain structure is not very proper for producing 3D models. Also, because UAVs are the mechanisms that are densely affected by wind, high-intensity wind may cause the expected accuracy to be not achieved.

In this study, the effect of flight height, overlap rate, and UAV type on the model investigated, and significant results gained. It has presented to the literature as an essential reference for future studies. Results and findings were discussed and concluded as an article for researchers.

ACKNOWLEDMENT

This Project supported by Selçuk University Scientific Research Projects with 18401080 project ID.

This study was made from Hasan Bilgehan Makineci's doctoral thesis titled "*Photogrammetric Based Image Acquisition and Flight Optimization by Unmanned Aerial Vehicle*".

REFERENCES

Akgul, M, Yurtseven H, Gulci S, Akay A E (2018). "*Evaluation of UAV-and GNSS-based DEMs for earthwork volume*." Arabian Journal for Science and Engineering 43.4: 1893-1909.

Ahn, S, and Jeffrey A. F. (2003). "*Standard errors of mean, variance, and standard deviation estimators*." EECS Department, The University of Michigan, 1-2.

Amukele, T. K., Sokoll, L. J., Pepper, D., Howard, D. P., & Street, J. (2015). Can unmanned aerial systems (drones) be used for the routine transport of chemistry, hematology, and coagulation laboratory specimens?. *PloS one*, *10*(7), e0134020.

Arik, S, Turkmen I, and Oktay T. (2018). "*Redesign of morphing UAV for simultaneous improvement of directional stability and maximum lift/drag ratio*." Advances in Electrical and Computer Engineering 18.4: 57-63.

Berni, J. A., Zarco-Tejada, P. J., Suárez, L., & Fereres, E. (2009). Thermal and narrowband multispectral remote sensing for vegetation monitoring from an unmanned aerial vehicle. *IEEE Transactions on geoscience and Remote Sensing*, *47*(3), 722-738.

Carr, B. B., Clarke, A. B., Arrowsmith, J. R., Vanderkluysen, L., & Dhanu, B. E. (2019). The emplacement of the active lava flow at Sinabung Volcano, Sumatra, Indonesia, documented by structure-from-motion photogrammetry. *Journal of Volcanology and Geothermal Research*, *382*, 164-172.

Clapuyt, F., Vanacker, V., & Van Oost, K. (2016). Reproducibility of UAV-based earth topography reconstructions based on Structure-from-Motion algorithms. *Geomorphology*, *260*, 4-15.

Comert, R., Avdan, U., Gorum, T., & Nefeslioglu, H. A. (2019). Mapping of shallow landslides with object-based image analysis from unmanned aerial vehicle data. *Engineering Geology*, *260*, 105264.

Colomina, I., & Molina, P. (2014). Unmanned aerial systems for photogrammetry and remote sensing: A review. *ISPRS Journal of photogrammetry and remote sensing*, *92*, 79-97.

Cryderman, C., Mah, S. B., & Shufletoski, A. (2014). Evaluation of UAV photogrammetric accuracy for mapping and earthworks computations. *Geomatica*, *68*(4), 309-317.

Draeyer, B., & Strecha, C. (2014). White paper: How accurate are UAV surveying methods. *Pix4D White Paper*.

Gaikwad, L. M., Teli, S. N., Majali, V. S., & Bhushi, U. M. (2016). An application of Six Sigma to reduce supplier quality cost. *Journal of The Institution of Engineers (India): Series C*, *97*(1), 93-107.

Govender, N. (2009). "*Evaluation of feature detection algorithms for structure from motion*."

Makineci, H. B., and Karabörk H. (2016). "*Evaluation Digital Elevation Model Generated by Synthetic Aperture Radar Data*." International Archives of the Photogrammetry, Remote Sensing & Spatial Information Sciences 41.

Makineci, H. B., Karabörk, H., & Durdu, A. (2020). "*The Performance Evaluation of Image Matching Techniques within UAV Images*", Turkish Journal of Geosciences, 1(1), 8-14.

Martínez-Carricondo, P., Agüera-Vega, F., Carvajal-Ramírez, F., Mesas-Carrascosa, F. J., García-Ferrer, A., & Pérez-Porras, F. J. (2018). Assessment of UAV-photogrammetric mapping accuracy based on variation of ground control points. *International journal of applied earth observation and geoinformation*, *72*, 1-10.

Mesas-Carrascosa, F. J., Notario-García, M. D., de Larriva, J. E. M., de la Orden, M. S., & Porras, A. G. F. (2014). Validation of measurements of land plot area using UAV imagery. *International Journal of Applied Earth Observation and Geoinformation*, *33*, 270-279.

Micheletti, N, Jim H. C, and Stuart N. L. (2015). "*Structure from motion (SFM) photogrammetry*."

Sabins, F F. (2007). "*Remote sensing: principles and applications*." Waveland Press.

Strecha, C. (2014). "*The rayCloud–a vision beyond the point cloud*." FIG Congress.

Uysal, M, Yılmaz, M, Tiryakioğlu, İ, Polat, N. (2018). İnsansız hava araçlarının afet yönetiminde kullanımı. Eskişehir Teknik Üniversitesi Bilim ve Teknoloji Dergisi B - Teorik Bilimler, 6, 219-224.

Thiels, C. A., Aho, J. M., Zietlow, S. P., & Jenkins, D. H. (2015). Use of unmanned aerial vehicles for medical product transport. *Air medical journal*, *34*(2), 104-108.

Yurtseven, H. (2019). "*Comparison of GNSS-, TLS-and different altitude UAV-generated datasets on the basis of spatial differences*." ISPRS International Journal of Geo-Information 8.4: 175.

Appendix

GCP Point List

POİNT ID	X (M)	Y (M)	ELEVATİON –Z- (M)
GCP100	540854,542	4183107,795	1143,539
GCP101	540853,665	4183221,507	1131,689
GCP102	541014,765	4183191,321	1144,026
GCP103	541038,158	4183080,744	1175,361
GCP104	540991,314	4183076,072	1181,547
GCP105	541033,735	4183346,319	1120,467
GCP106	540856,488	4183389,589	1117,526
GCP107	540690,984	4183028,012	1126,198
GCP108	540680,933	4183190,195	1117,285